Symmetry in the diffraction of beams carrying orbital angular momentum

Anindya Ambuj,[1] Emily Walla,[1,2] Sophia Andaloro,[1,3] Sean Nomoto,[1] Reeta Vyas,[1] and Surendra Singh[1,*]
[1]*Department of Physics, University of Arkansas, Fayetteville, Arkansas 72701, USA*
[2]*Department of Physics and Department of Astronomy, University of Arizona, Tucson, Arizona 85721, USA*
[3]*Physics Department, University of Dallas, Dallas, Texas 75062, USA*

(Received 22 October 2018; published 24 January 2019)

Diffraction of orbital-angular-momentum–carrying Laguerre-Gauss vortex (LGV) beams by N-fold rotationally symmetric regular polygons is studied analytically and experimentally. The structure, symmetry, and dependence of the diffraction pattern on the angular momentum index of the LGV beam and the number of sides in the polygon are systematically investigated, and features and trends are identified. The evolution of the diffraction pattern and its symmetry with the aperture position relative to the waist is also studied, leading to a generalized Friedel's law for diffraction of LGV beams.

DOI: 10.1103/PhysRevA.99.013846

I. INTRODUCTION

Diffraction is a common occurrence when a wave field encounters an obstacle. Far-field or Fraunhofer diffraction of plane waves from two-dimensional objects such as an aperture is of particular interest, of which many examples can be found in textbooks [1,2]. It is well known that the Fraunhofer diffraction is the Fourier transform of the incident field distribution in the plane of the aperture multiplied by the aperture transmission function [3]. For an incident plane wave, the field in the plane of the aperture is a constant. The structure of the diffracted field is then determined by the shape and symmetry of the aperture. Of course, the aperture, in general, has a lower symmetry than the diffraction field. In inverse problems, the relation between the symmetry of the diffracted field and structure of the scatterer is of interest in all branches of diffraction physics [4–7]. Plane-wave diffraction by regular polygonal apertures has been treated in a number of classic papers, which among other things, show that the diffraction pattern has the same rotational and mirror symmetries as the aperture transmission function [8–11]. For an incident field with a more complex spatial profile than a plane wave, the structure of the diffracted field is no longer determined solely by the symmetry of the aperture transmission function. Of particular interest are the so-called Laguerre-Gauss vortex (LGV) beams, which are solutions to the paraxial scalar wave equation in circular cylindrical coordinates [12–15]. The LGV beams have a helicoidal phase front with a phase singularity (field null) along the beam axis, where the spatial dependence can be written as $\rho^{\ell} e^{i\ell\varphi}$, with ℓ a positive or negative integer or zero. These beams carry intrinsic orbital angular momentum (OAM) of $\ell\hbar$ per photon. The integer ℓ is referred to as the OAM index of the beam. With their new degree of freedom in OAM, the LGV beams have inspired new thinking in many light-matter-interaction processes and found novel applications [16–19]. Studies of scattering of LGV beams by simple apertures have revealed many unexpected features in the diffraction pattern [20–25] and interesting implications for the relationship between the symmetries of the diffraction pattern and the scattering object [7,26–28]. These investigations used slits, triangular or square apertures, or their combination to study diffraction, primarily as a tool to determine the magnitude and sign of the OAM index and much less to study the symmetry in diffraction [27,28]. In this paper we present a systematic theoretical and experimental investigation of the interaction between discrete geometrical symmetries of regular polygonal apertures and the OAM of an incident LGV beam and how it constraints the symmetry of the diffraction pattern. We discuss the structure, symmetry, and trends in the diffraction pattern as N and ℓ are varied. We also discuss how these features evolve as the longitudinal position of the aperture is changed relative to the beam waist and present experimental evidence for theoretical conclusions [29].

II. THEORY

Consider a two-dimensional N-sided regular polygonal aperture $\mathcal{A}$ in an opaque plane screen occupying the x'-y' plane illuminated by a monochromatic field incident from $z < 0$. Throughout the paper we will consider the transmission function of the aperture to be real. The spatial part of the Fraunhofer field E_f, observed by placing the aperture in the front focal plane of a lens of focal length f and the detector in the back focal plane (see the experimental setup in Fig. 4), is given by [3]

$$E_f(x, y; z) = \frac{ik}{2\pi f} \iint d\mathcal{A} E_{in}(x', y', z)\, e^{-\frac{ik}{f}(xx'+yy')}, \qquad (1)$$

where $E_{in}(x', y', z)$ represents the spatial part of the incident wave field in the aperture plane at a distance z from the waist of the incident beam, $k = 2\pi/\lambda$ is the wave number, λ being the wavelength of light, x', y' are the transverse coordinates of a point in the aperture plane, and x, y are the transverse coordinates of a point in the back focal plane of the lens.

*Corresponding author: ssingh@uark.edu

For an incident LGV beam (zero radial index) traveling in direction z, the complex field amplitude is given by

$$E_{in}^{(\ell)}(x', y', z) = \text{const} \times \rho'^{|\ell|} e^{ikz - i(|\ell|+1)\theta} \times \exp\left[i\ell\varphi' - \frac{\rho'^2}{w w_o} e^{-i\theta} \right], \quad (2)$$

where $\rho' = \sqrt{x'^2 + y'^2}$ and $\varphi' = \tan^{-1}(y'/x')$ are the radial and angular coordinates of a point in a plane transverse to the direction of propagation, $z_R = \pi w_o^2/\lambda$ is the Rayleigh range, $w \equiv w(z) = w_o\sqrt{1 + z^2/z_R^2}$ is the spot radius, which has its minimum value w_o at the beam waist $z = 0$, and $\theta \equiv \theta(z) = \tan^{-1}(z/z_R)$ is the Guoy's phase of the beam. The factor $e^{i\ell\varphi'}$ describes the azimuthal variation of the phase responsible for the helical twist of the phase front. The OAM index ℓ is also referred to as the topological charge of the vortex.

For an analytic description, we take the aperture transmission to be unity over the extent of the aperture $\mathcal{A}$ and zero outside, and the LGV beam to be incident normally and beam axis to pass through the center of the aperture. Then, using polar coordinates ρ', φ' for the aperture plane and ρ, φ for the observation plane, the diffraction integral can be written as

$$E_\ell(\rho, \varphi; z) = C_\ell \iint_{\mathcal{A}} d\rho' d\varphi' \rho'^{|\ell|+1} \times e^{i\ell\varphi' - \frac{\rho'^2}{w w_o} e^{-i\theta} - i(\frac{k\rho\rho'}{f})\cos(\varphi - \varphi')}, \quad (3)$$

where the factor $e^{ikz - i(|\ell|+1)\theta(z)}$, which does not depend on the variables of integration, has been absorbed into the constant C_ℓ and the aperture $\mathcal{A}$ is a regular polygonal of side N, which has N-fold rotational symmetry and N mirror lines. Before proceeding further, we can draw several general conclusions regarding the diffraction pattern by examining the structure of the diffraction integral (3) for an LGV beam.

We note that for $\ell = 0$ and $w \to \infty$, the integral reduces the plane-wave diffraction by polygonal apertures considered in earlier investigations [8–11]. In this case, the diffraction field reflects the symmetries of the aperture. In addition, the diffraction profile [$\propto |E_f(\rho, \varphi; z|^2)$] has a center of inversion, even if the aperture lacks one [5]. In contrast, for an LGV beam ($\ell \neq 0$), because of the azimuthal variation of the phase of the incident field, the integrand does not have a center of inversion. This can be seen by comparing $E_\ell(\rho, \varphi; z)$ to its complex conjugate $E_\ell^*(\rho, \varphi; z)$ and recalling $\cos(\phi + \pi) = -\cos\phi$. This leads to the relation

$$|E_\ell(\rho, \varphi; z)|^2 = |E_{-\ell}(\rho, \varphi + \pi; -z)|^2, \quad (4)$$

where we have used $|E_\ell|^2 = |E_\ell^*|^2$. Equation (4) implies that, in general, the LGV diffraction patterns do not have a center of inversion. For the special case of an aperture at beam waist $z = 0$, this reduces to the result derived in Refs. [7,26], according to which the diffraction patterns for LGV beams of indices ℓ and $-\ell$ from two-dimensional apertures with real transmission function are related by a rotation of π (centrosymmetric in two dimensions). For aperture positions away from the waist, the diffraction patterns for $\pm\ell$ produced by the aperture are not centrosymmetric to one another. Instead, the pattern for ℓ with the aperture at z and the pattern for $-\ell$ with the same aperture at $-z$ are related by a rotation of π. Reverting back to Cartesian coordinates, the relation (4) can be written as $|E_\ell^*(x, y; z)|^2 = |E_{-\ell}(-x, -y; -z)|^2$, which shows that the patterns for ℓ and $-\ell$ are not centrosymmetric in two dimensions, but they are related by a three-dimensional inversion through the center of the beam in the waist plane. Equation (4) is thus the generalized Friedel law for diffraction of LGV beams by two-dimensional apertures. To avoid confusion, we will use centrosymmetric in the rest of paper in the sense of inversion through origin in two dimensions ($x, y \to -x, -y$). We return to this point later in the discussion of the experimental results.

It is important to mention here that the symmetry condition implied by Eq. (4) holds not only for the LGV beams given by Eq. (2) (Laguerre-Gauss beams of zero radial index), but also for more general types of angular-momentum–carrying beams. For example, if we use the expression for the field of a Laguerre-Gauss beam of nonzero radial index [13], which differs from Eq. (2) by the multiplicative factor $L_p^\ell[2\rho^2/w(z)]\exp[-i2p\theta(z)]$, in the diffraction integral, we again arrive at Eq. (4). Another class of orbital-angular-momentum–carrying beams are the so-called Bessel-Gauss beams [30,31]. Using the field of these beams, we can again show that the relation (4) holds.

More generally, the z-dependent aspect of relation (4) will be important not only for OAM-carrying beams, but for all paraxial beams diffracted by real apertures. To see this, we consider the free-space paraxial wave equation for the (scalar) field amplitude

$$\left[\frac{\partial^2}{\partial x^2} + \frac{\partial^2}{\partial y^2} + 2ik\frac{\partial}{\partial z} \right] E(x, y, z) = 0. \quad (5)$$

By comparing this to the equation for the complex conjugate of the field amplitude, we find that the complex field amplitude satisfies the condition

$$E^*(x, y, -z) = e^{i\phi_o} E(x, y, z), \quad (6)$$

where ϕ_o is some constant phase. As a check, all the well-known paraxial laser beam families Laguerre-Gauss, Hermite-Gauss, Ince-Gauss, Bessel-Gauss, and Airy beams [13,30–33] satisfy this condition. By taking the incident field E_{in} in Eq. (1) to be that of a paraxial beam, which satisfies Eq. (6), we find that the diffracted field from real apertures satisfies

$$E_f^*(-x, -y; -z) = -e^{i\phi_o} E_f(x, y; z) \quad (7)$$

and

$$|E_f^*(-x, -y; -z)|^2 = |E_f(x, y; z)|^2. \quad (8)$$

Equation (8) is the generalized Friedel's law for paraxial laser beams, which for LGV beams leads to Eq. (4).

For idealized beams where the dependence of the field amplitude on the transverse coordinates and the z coordinate (coordinate in the direction of propagation) can be factorized as, for example, for nondiffracting Bessel beams [34], Eq. (4) reduces to $|E_\ell(\rho, \varphi)|^2 = |E_{-\ell}(\rho, \varphi + \pi)|^2$.

To continue with our analytical treatment, we consider the polygon to be inscribed in a circle of radius R, label its N vertices, counterclockwise, $0, 1, 2, \ldots, N-1$, and choose the x' axis to pass through the vertex labeled 0 and y' axis perpendicular to it as shown in Fig. 1. The integral can then be written as the sum of integrals over N congruent isosceles triangles. The base (b) and height (h) of isosceles

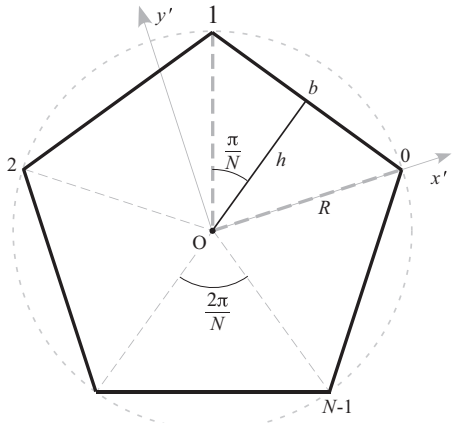

FIG. 1. Coordinate system for the polygonal aperture.

triangles, and the angular coordinates of the vertices (φ_n) and the midpoints of the sides ($\varphi_{n+\frac{1}{2}}$) of the polygon, are given by

$$h = R\cos(\pi/N), \quad b = 2R\sin(\pi/N), \quad \varphi_n = \frac{2\pi n}{N}, \qquad \varphi_{n+\frac{1}{2}} = \frac{\pi(2n+1)}{N}, \quad n = 0, 1, \ldots, (N-1), \tag{9}$$

and the nth triangle occupies the angular range $\varphi_n \leqslant \varphi' \leqslant \varphi_{n+1}$. Then the diffracted field can be written as the contribution from N triangles,

$$E_\ell(\rho, \varphi; z) = C_\ell \sum_{n=0}^{N-1} \int_{\varphi_n}^{\varphi_{n+1}} d\varphi' \int_0^{\rho_m(\varphi')} d\rho' \rho'^{|\ell|+1} \times e^{i\ell\varphi' - (\frac{e^{-i\theta}}{ww_o})\rho'^2} e^{-i\kappa\rho'\cos(\varphi-\varphi')}, \tag{10}$$

where the abbreviation $\kappa = k\rho/f$ has been introduced and $\rho_m(\varphi') = \frac{h}{\cos(\varphi'-\varphi_{n+\frac{1}{2}})}$ is the maximum height of a wedge of angular width $d\varphi'$ located around φ'. By introducing a local angular variable ϕ' relative to the midpoint of the base of the nth triangle by

$$\phi' = \varphi' - \varphi_{n+\frac{1}{2}}, \quad -\pi/N \leqslant \phi' \leqslant \pi/N, \tag{11}$$

the diffracted field can be written as

$$E_\ell(\rho, \varphi; z) = C_\ell \sum_{n=0}^{N-1} e^{i\ell\varphi_{n+\frac{1}{2}}} \int_{-\pi/N}^{\pi/N} d\phi' e^{i\ell\phi'} \int_0^{\rho_m(\phi')} d\rho' \times \rho'^{|\ell|+1} e^{-(\frac{e^{-i\theta}}{ww_o})\rho'^2} e^{-i\kappa\rho'\cos(\varphi-\varphi_{n+\frac{1}{2}}-\phi')}, \tag{12}$$

with

$$\rho_m(\phi') = \frac{h}{\cos\phi'}. \tag{13}$$

Thus the diffracted field is the superposition of fields produced by N isosceles triangle sources with the epoch angle varying, counterclockwise, in steps of $2\pi\ell/N$, starting with $\pi\ell/N$ for $n = 0$. Additional contribution to the phase comes from the integral as it yields, in general, a complex quantity that depends on ρ, φ, n, and N. As a quick check of this form, we see that in the limit $N \to \infty$, with $2\pi/N \to d\psi$, $\varphi_{n+\frac{1}{2}} \to \psi$, and $\rho_m = h/\cos\phi' = R\cos(\pi/N)/\cos\phi' \to R$, we get

$$E_\ell(\rho, \varphi; z) = C_\ell \frac{e^{i\ell\varphi}}{2\pi} \int_0^{2\pi} d\psi e^{-i\ell(\varphi-\psi)} \int_0^R d\rho' \rho'^{|\ell|+1} \times e^{-(\frac{e^{-i\theta}}{ww_o})u^2 - i\kappa u\cos(\varphi-\psi)} = C_\ell e^{i\ell\varphi} \int_0^R d\rho' \rho'^{|\ell|+1} e^{-(\frac{e^{-i\theta}}{ww_o})u^2} J_\ell(\kappa u), \tag{14}$$

which is the correct limit for diffraction from a circular aperture of radius R [25].

Returning to Eq. (12), the dependence on n via $\varphi_n + \frac{1}{2}$ in each term in Eq. (12) can be factored out by expanding the exponential $e^{-i\kappa\rho'\cos(\varphi-\varphi_{n+\frac{1}{2}}-\phi')}$ in a series of Bessel functions [35]. The sum with respect to n can then be performed, leading us to

$$E_\ell(\rho, \varphi; z) = C_\ell \sum_{p=-\infty}^{\infty} (-1)^{|p|}(-i)^{|pN-\ell|} e^{-i(pN-\ell)\varphi} \times \int_{-\pi/N}^{\pi/N} d\phi' e^{ipN\phi'} \int_0^{\rho_m(\phi')} d\rho' \rho'^{|\ell|+1} \times e^{-(\frac{\rho'^2}{ww_o})} e^{-i\theta} J_{|pN-\ell|}(\kappa\rho'). \tag{15}$$

A careful inspection of this expression shows that a Bessel function of order zero occurs in this series only when $|pN - \ell| = 0$ for some p, i.e., when the OAM index ℓ is an integer multiple of N. This, in turn, means that the center ($\rho = 0$) of the diffraction pattern will be bright if ℓ is a multiple of N and dark for all other values of ℓ, since a Bessel function of order other than zero vanishes at the origin, $J_m(0) = 0$ ($m \neq 0$). By utilizing the small argument expansion of Bessel functions near the axis ($\rho \to 0$), we can see that even when ℓ is a multiple of N, the intensity at the center decreases as $1/N^2$ so that in the limit of a circular aperture ($N \to \infty$) the center is always dark [25].

For numerical evaluation of the diffraction patterns, the radial integral in Eq. (12) can be expressed in terms of an incomplete Γ function [36], which is a built-in function in many computer programs. In practice, it is more efficient to evaluate the diffraction integral directly as a two-dimensional fast Fourier transform (FFT) using MATLAB or MATHEMATICA using the results derived here as checks to ensure the accuracy against any numerical artifacts.

Figure 2 shows the diffraction patterns computed by evaluating the diffraction integral (3) using the FFT in MATLAB for $N = 3, 4, 5$ and different ℓ when the aperture is at beam waist, where the incident beam phase fronts are planar with $\theta(0) = 0$, $w(0) = w_o$. These calculations were carried out by choosing the radius of the irradiance maximum to be equal to the radius of the circle circumscribing the polygon. This is similar to the condition under which the experiments described later in the paper were carried.

First we note that the diffraction patterns from an N-sided polygonal have N-fold rotational symmetry, reflecting the symmetry of the aperture. Thus the patterns for $N = 3, 4, 5$ have, respectively, three-, four-, and fivefold rotational symmetry. Second, for polygons with an odd number of sides ($N = 3$ and 5 in Fig. 2), the diffraction pattern lacks a center

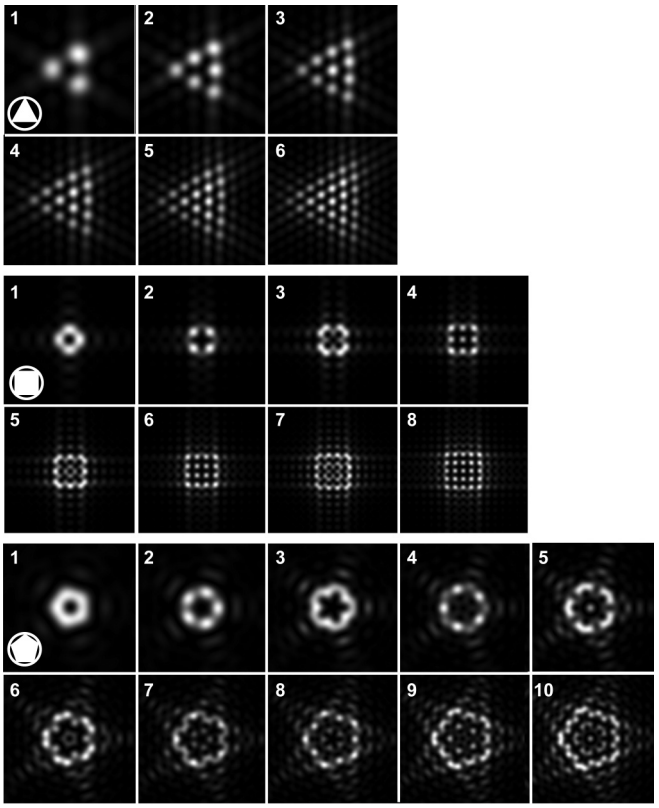

FIG. 2. Irradiance patterns in the diffraction of LGV beams by an equilateral triangle ($N = 3$), square ($N = 4$), and pentagon ($N = 5$) placed at the beam waist for ℓ values as indicated in the image frames. The lower left corner of the image frames labeled 1 shows the orientation of the apertures.

of inversion, whereas for polygons with an even number of sides ($N = 4$ in Fig. 2), it has a center of inversion. This is in contrast to the diffraction of a plane wave, where the diffraction pattern always has a center of inversion even if the aperture does not [5].

By examining the evolution of the diffraction pattern with OAM index ℓ for fixed N, we find that the diffraction pattern has a null at the center for all values of ℓ except when ℓ is a multiple of N. For example, for $N = 3$, the patterns have a bright center for $\ell = 0, 3, 6, \ldots$ and a dark center for $\ell = 1, 2, 4, 5$. Similarly, for $N = 4$, the center is bright for $\ell = 0, 4, 8 \ldots$, dark for $\ell = 1, 2, 3, 5, 6, 7$, and for $N = 5$ the center is bright for $\ell = 5, 10, 15 \ldots$ and dark in all other cases.

Focusing now on the diffraction pattern in the central region, where most of the diffracted light is concentrated, we observe that the patterns have a nested structure—the central feature of the pattern for $\ell > N$ is the pattern for $\ell - N$. This is most clearly seen in the patterns for $N = 3$, where the central feature of the pattern for $\ell = 4$ is the pattern for $\ell = 1 (= 4 - 3)$, and the central feature of the pattern for $\ell = 5$ is the pattern for $\ell = 2 (= 5 - 3)$. Likewise, the central feature for $\ell = 7$ is the pattern for $\ell = 4 (= 7 - 3)$, which in turn encloses the pattern for $\ell = 1 (= 4 - 3)$. This nesting pattern is present in the diffraction by polygons with $N > 3$ as well, although it is not as well resolved as in the

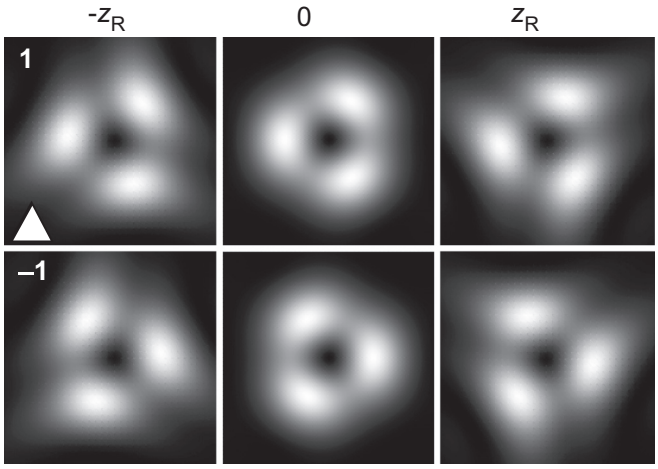

FIG. 3. Evolution of the diffraction of an $\ell = 1$ LGV beam by a triangular aperture as the aperture position is varied from one side of the waist ($z = -z_R$) to the other ($z = z_R$).

case of small N. Certain broad features of the diffraction pattern can be understood by considering the diffraction to be an interference of waves diffracted by the edges of the polygon. This has been discussed for a triangular $N = 3$ aperture yielding a triangular lattice of bright spots [22,23,37]. A similar approach for a square aperture can be seen to lead to the square-lattice-like structure seen for $N = 4$ patterns. Successively larger values of ℓ reveal correspondingly larger portions of triangular, square, and other types of lattices formed by the interference of edge-diffracted waves.

For aperture positions away from the waist, the incident phase front in the aperture plane has a radially varying phase and a z-dependent Guoy's phase, resulting in a significantly altered diffraction pattern. This is shown in Fig. 3, which compares the diffraction patterns for a triangle ($N = 3$) aperture at the waist ($z = 0$) and one Rayleigh range away ($\pm z_R$) from the waist. The patterns have N-fold rotational symmetry for all aperture positions, but only at the waist are the patterns for $-\ell$ and ℓ related by a rotation of 180°. Away from the waist, the pattern for ℓ at z is related to the pattern for $-\ell$ at $-z$ by a rotation of 180°, in agreement with Eq. (4). In going from $z = 0$ to z_R, the patterns rotate and outer portions of the pattern acquire a shear. The sense of rotations for positive and negative ℓ are opposite and, the shear, evident in the outer portions of the pattern, depends on the sign of z reflecting its origin in Guoy's phase.

III. EXPERIMENT

These features of the LGV diffraction from polygonal apertures are readily observed by illuminating polygonal apertures with LGV beams. The LGV beams were created by diffracting a collimated fundamental Gaussian beam from a spatial light modulator (SLM) controlled by a computer (see Fig. 4). The computer could be programmed to write the phase grating of any desired LGV mode on the sensitive surface of the SLM. The LGV beams with different OAM index were produced in reflected light. An appropriately placed aperture after the SLM selected an LGV beam of desired OAM index and blocked

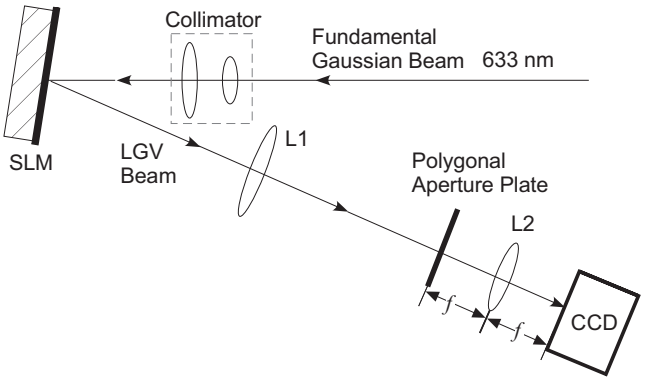

FIG. 4. An outline of the experimental setup.

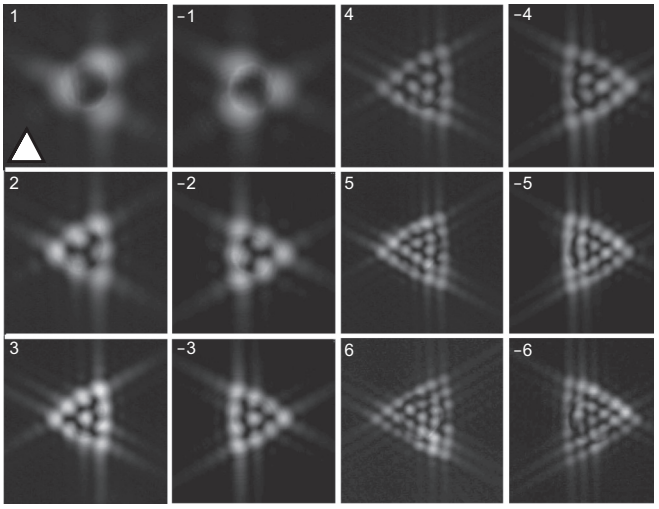

FIG. 5. Recorded LGV diffraction irradiance from a regular triangular aperture ($N = 3$) at the beam waist for ℓ values as indicated in the frames. Frames for $\pm\ell$ have been paired for easy comparison.

the unwanted beams. The LGV beams with OAM index up to $\ell = 10$ were produced this way. Figure 4 shows an outline of the experimental setup used for observing the diffraction of LGV beams by regular polygonal apertures.

Lens L1 forms a waist of the LGV beam. A second lens L2 was placed, downstream from L1, such that the aperture was in its front focal plane and a CCD camera in its back focal plane. This arrangement, known as "$2f$" arrangement, ensures that the CCD camera records the far-field (Fraunhofer) diffraction [3]. In the experiment, the aperture-L2-CCD combination was moved as a single unit along the beam axis, without changing the relative distances between the three elements. This allowed the aperture to be placed at any position relative to the beam waist along the beam axis and record the diffraction pattern.

In the experiment, it was necessary to control the location of the beam waist and the fundamental Gaussian beam spot radius w_o. This is because the irradiance pattern of the LGV beam consists of single bright ring whose radius w_m is given by $w_m = \sqrt{\ell + 1}\, w_o$, where ℓ is the OAM index of the beam and minimum spot radius w_o of the fundamental ($\ell = 0$) Gaussian beam [38]. Thus as the OAM index of the LGV beam increases, the radius of the irradiance maximum also increases. This means that in studies of ℓ dependence of diffraction, as ℓ increases the size of the maximum irradiance ring may grow so large that the polygon interacts essentially with the low-intensity core of the beam, making the recording of the pattern difficult. Furthermore, the apertures were etched on a glass plate coated with a thin layer of chrome, and when the radius of irradiance maximum exceeded the aperture size, a significant beam leaked through the glass plate to overwhelm the diffraction pattern. For this reason, the experiments were conducted with $w_m \approx R$, where R is the radius of the circle circumscribing the polygon. This also means that the spatial scales in recorded diffraction patterns are not directly comparable, but it allows recording of the structure of diffraction pattern, which is our main interest. For this purpose, several different lenses with focal lengths ranging from 35 to 75 cm were used for L1, allowing us to create a beam radius w_o varying from from 150 to 400 μm. The LGV beams generated were collimated, placing the beam waist after the lens L1 nominally in the back focal plane of the lens. For locating the waist plane more accurately, a CCD camera was used, which also allowed a determination of the radius w_m of the maximum intensity ring of the LGV beam.

The experiments were carried out first by placing the apertures at beam waist and illuminating them with LGV beams with different values of OAM index ℓ. Then the aperture position was varied relative to the waist of the beam to study the effects of the LGV beam's quadratic radial phase profile and Gouy's phase on diffraction.

IV. RESULTS AND DISCUSSION

Figure 5 shows the recorded irradiance patterns resulting from the diffraction of LGV beams of different OAM index ℓ from an equilateral triangular aperture placed at the waist of the incident beam. These experimentally recorded patterns agree with the corresponding theoretical patterns of Fig. 2. In particular, they lack a center of inversion, display a nested structure as a function of ℓ, and have a bright center for $\ell = \pm 3$ and ± 6, i.e., when ℓ is a multiple of N, and a dark center for all other values of ℓ.

In the experiment, LGV beams of both positive and negative ℓ values were used. These are also shown in Fig. 5. The patterns for OAM index $\pm\ell$ are related by a rotation of 180°, as predicted by Eq. (4) for aperture position at the beam waist ($z = 0$).

In carrying out the experiment, the intensity of the incident beam had to be adjusted from one frame to another so as not to saturate the detector. For this reason the intensities in different frames are not directly comparable. In some cases, detector saturation could not be avoided over the entire frame. In such cases, the saturated regions appear as red in the grayscale images. The slight curvature seen in diffraction images for higher ℓ values is not a detector artifact but a property of the diffraction pattern itself. As mentioned in the discussion of the experiment in Sec. III, the experiments were carried out by adjusting the radius $w_m = w_o\sqrt{\ell + 1}$, where the incident beam has maximum irradiance, to be nearly equal to the radius R of the circle circumscribing the polygon. This

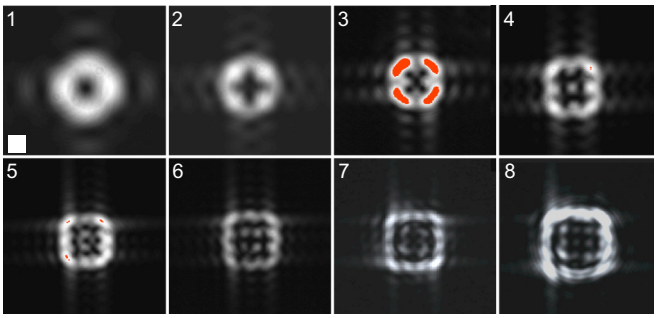

FIG. 6. Recorded LGV diffraction patterns from a square aperture ($N = 4$) at the beam waist for positive ℓ values as indicated in the frames.

curvature effect is enhanced for w_m values smaller than R and is suppressed for $w_m > R$. Numerical evaluations can reproduce this effect as well. Evidence of this can be seen in the theoretically computed diffraction patterns shown in Fig. 2 for $\ell > 4$, in the case of a triangular aperture, and $\ell > 6$, in the case of a square aperture. These theoretical patterns were computed for $w_m = R$.

Figure 6 shows the recorded diffraction patterns for a square aperture illuminated by LGV beams of different OAM indices. All diffraction patterns have a fourfold rotational symmetry and a center of symmetry reflecting the symmetries of a square aperture. The patterns recorded for negative OAM index coincided with those for positive ℓ, in agreement with the implications of Eq. (4), and are not shown here. As a function of OAM index ℓ, the diffraction patterns for $\ell = 1$–4 are distinct and shown in the top row. For $\ell > 4$, the patterns have a nested structure: the pattern for $\ell = 5$ has an $\ell = 1$ pattern as its core, the $\ell = 6$ pattern has an $\ell = 2$ pattern as its core, and so on. Although the core evolves with ℓ somewhat, in general appearance, the pattern for $\ell > N$ has the pattern for $\ell - N$ as its core. Finally, we note that the patterns for $\ell = 4$ and $\ell = 8$ have a bright center, in agreement with the discussion following Eq. (15). These profiles agree with the theoretical profiles in Fig. 2 for $N = 4$.

Diffraction patterns for LGV beams with $-5 \leqslant \ell \leqslant 5$ scattered from a regular pentagon ($N = 5$) at the beam waist are shown in Fig. 7. The patterns for $\pm\ell$, paired together for ease of comparison, are centrosymmetric to one another. The last two frames for $\ell = \pm 10$ also obey this relation. Additionally, together with the $\ell = \pm 5$ frames, they illustrate that the center of the diffraction pattern is bright when ℓ is a multiple of N. They also exhibit a nested structure observed for $N = 3$ and $N = 4$ apertures. Similar patterns were recorded for apertures with $N = 6 - 9$, and in all cases they confirm the structures and trends predicted in the preceding section.

So far, we have studied diffraction patterns for the apertures placed at the beam waist, where the LGV beam phase fronts are planar and, for normally incident beams, the phase in the plane of the aperture is constant. Away from the waist, the phase fronts are spherical—the phase has a quadratic radial dependence as well as a dependence on z via the Guoy's phase. Because of these two additional phase contributions, the diffraction patterns of LGV beams evolve as the aperture is moved away from the waist.

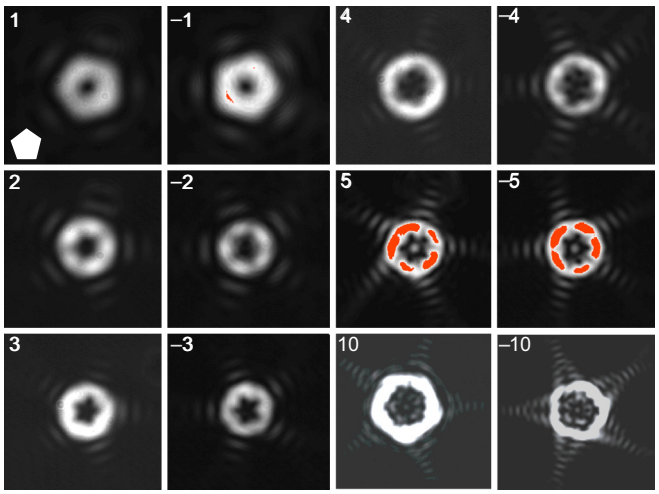

FIG. 7. Recorded LGV diffraction patterns from a regular pentagon ($N = 5$) at the beam waist for ℓ values as indicated in the frames.

Figure 8 shows an experimentally recorded evolution of diffraction patterns for triangular and square apertures as their position is varied from $-z_R$ to z_R relative to the beam waist

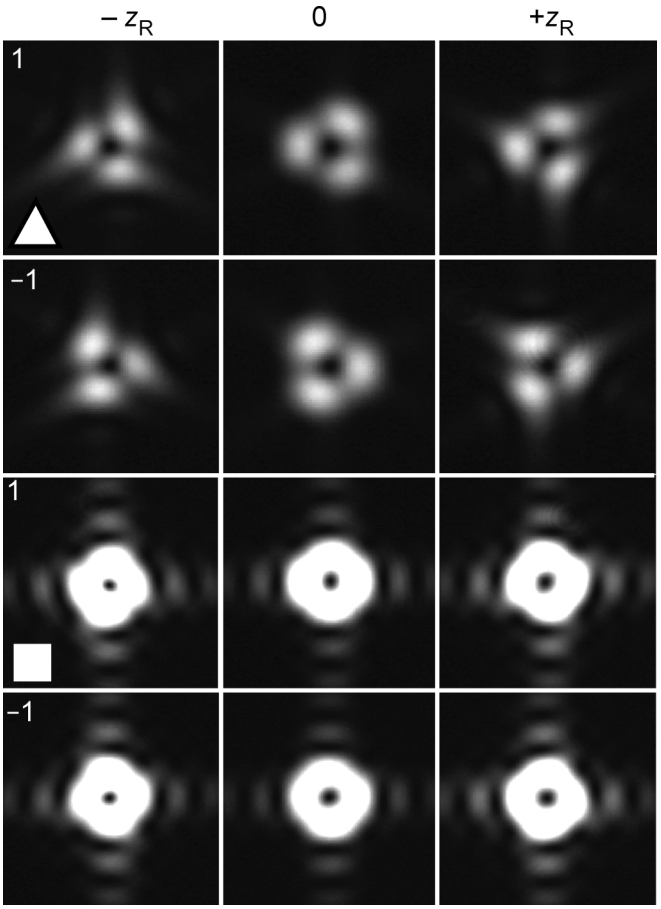

FIG. 8. Recorded LGV diffraction patterns from triangle and square apertures placed at $z = -z_R$, 0 and z_R as indicated for $\ell = \pm 1$. The top two rows are for a triangular aperture and the bottom two for a square aperture. The lower left corner of frames labeled 1 show the orientation of the apertures.

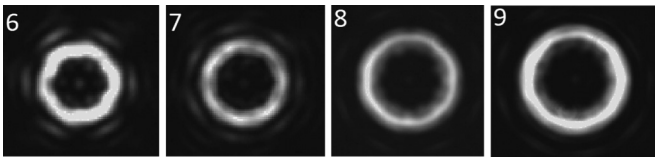

FIG. 9. Recorded LGV diffraction patterns from polygonal apertures placed at $z = 0$ for $\ell = N$ as indicated.

$z = 0$. Note that these patterns show a rotation as well as a shear as the apertures move from $-z_R$ to z_R. While the rotation of the patterns continues monotonically in the same sense (depending on the sign of ℓ) in crossing the waist, the sense of shear reverses in crossing the waist. The ℓ-dependent rotation is caused by the Guoy's phase dependence on the OAM index of the beam, while the shear of the pattern is caused by the quadratic radial dependence of the phase of the incident beam [24,26]. For all positions, the patterns for the triangle and square have, respectively, threefold and fourfold rotational symmetry. For the square, they all have a center of inversion, whereas for $N = 3$ they lack a center of inversion.

We note also that for both apertures, when they are placed at the waist ($z = 0$), the $\ell = \pm 1$ diffraction patterns are 180° rotated versions of one another. This relation breaks down for aperture positions away from the waist. This breakdown is most apparent in the sense of shear in the outer portions of the patterns. For example, a comparison of the ± 1 patterns for a triangle at $z = -z_R$ shows that a 180° rotation of $\ell = -1$ pattern may get the main bright lobs to overlap with those in the $\ell = 1$ pattern but the sense of shear in the outer regions will be incorrect. On the other hand, a 180° rotated pattern for $\ell = -1$ at $z = -z_R$ will reproduce the pattern for $\ell = 1$ at $z = z_R$. Similar comments hold for the diffraction patterns produced by the square aperture. Thus when the apertures are placed one Rayleigh range away from the waist, the diffraction patterns for $\ell = \pm 1$ are not centrosymmetric to each other; rather, the pattern for $\ell = 1$ produced by the aperture placed at $z = z_R$ is centrosymmetric to the pattern for $\ell = -1$ produced by the aperture placed at $z = -z_R$. Thus the generalized relation for LGV diffraction embodied in Eq. (4) holds irrespective of the symmetry of the aperture as long as the aperture transmission function is real.

Conclusions regarding the symmetry of the diffraction pattern for Laguerre-Gauss beams of zero radial index considered in this paper will apply to Laguerre-Gauss beam of nonzero radial index as well, though the detailed spatial structure of the corresponding diffraction pattern will differ significantly from that for the LGV beams. This can be seen by recalling that the field of a nonzero radial index beam is obtained by multiplying the field of a pure vortex beam given in Eq. (2) by an appropriate associated Laguerre polynomial, which is a real function of the radial variable ρ [12,13], and this will not affect the argument used in arriving at Eq. (4).

We also studied the diffraction of LGV beams by polygons up to $N = 9$. As the number of sides increases, the diffraction patterns become increasingly similar to the diffraction by a circular aperture. Figure 9 shows the diffraction patterns produced by regular polygons with $N = 6$–9 for LGV beams of OAM index $\ell = N$. Increasing circular symmetry of the pattern as N increases is easily seen in these patterns. The bright spot in the center for the $\ell = N$ pattern is still present, but its intensity decreases as N increases, as noted in the discussion following Eq. (15). In the $N \to \infty$ limit, the aperture shape becomes a circle and, of course, the central bright spot disappears as the diffraction pattern becomes that of a circular aperture [25,39].

V. CONCLUSIONS

In conclusion, we have studied the diffraction of Laguerre-Gauss vortex beams from regular polygons (N-fold rotationally symmetric) analytically and experimentally. The dependence of diffraction on symmetry of the aperture, orbital-angular-momentum index ℓ, and aperture position relative to the beam waist has been investigated. For odd-N apertures, the diffraction lacks a center of inversion, whereas for even-N, it has a center of symmetry. Thus, overall, the diffraction pattern has the rotational as well as the inversion symmetry of the aperture. For apertures located at the waist, where the phase fronts are planar, the diffraction patterns for $\pm\ell$ are related by a rotation of 180°. For other locations of the aperture, this relationship no longer holds. Instead, a more general relation represented by Eq. (4) holds.

For fixed N, the patterns are distinct for $1 \leqslant \ell \leqslant N$, whereas for $\ell > N$, the central pattern displays a nested structure in that the central pattern for ℓ contains the pattern for $\ell - N$. This means that the pattern for $\ell > nN$ (n is a positive integer > 1) contains the patterns for $\ell - N$, which contains the pattern for $\ell - 2N$, and so on, the innermost pattern being that of $\ell - nN$.

For aperture positions away from the waist, diffraction is affected both by the quadratic radial dependence of phase and Guoy's phase contribution to it. Their effect is manifest in the overall rotation of the pattern and shear in the outer portions of the pattern. We also find that Eq. (4) represents an extension of Friedel's law for LGV beams, which itself is a special case of a more general symmetry relation (8) for the diffraction of paraxial beams by real apertures. It should be pointed out that Eq. (4) is not a consequence of the symmetry of the aperture; it is a property of paraxial vortex beams scattered by any two-dimensional apertures with real transmittance functions, independent of the symmetry of the aperture. Experimentally recorded diffraction profiles confirm analytically and numerically predicted structure and trends of the diffraction of LGV beams from regular polygonal apertures as functions of N and ℓ.

ACKNOWLEDGMENTS

Emily Walla and Sophia Andaloro were supported by the NSF-REU program (NSF Award No. 1460754) at the University of Arkansas. R.V. and S.S. acknowledge stimulating discussions on classical and quantum diffraction with Professor W. Schleich and support from the Center for Integrated Quantum Science and Technology (IQST) at Ulm University, Germany, where part of this work was completed.

[1] M. Born and E. Wolf, *Principles of Optics* (Cambridge University Press, New York, 1999), Chap. 8.

[2] F. A. Jenkins and H. E. White, *Fundamentals of Optics*, 3rd ed. (McGraw-Hill, New York, 1957), Chaps. 15–18.

[3] J. Goodman, *Introduction to Fourier Optics* (McGraw-Hill Book Company, New York, 1996).

[4] R. C. Smith and J. S. Marsh, Diffraction patterns of simple apertures, J. Opt. Soc. Am. **64**, 798 (1974).

[5] M. G. Friedel, Sur les symétries cristallines que peut réveiler la diffraction des rayons Rontgen, C. R. Seances Acad. Sci., Ser. A **157**, 1533 (1913).

[6] R. Juchtmans and J. Verbeeck, Orbital angular momentum in electron diffraction and its use to determine chiral crystal symmetries, Phys. Rev. B **92**, 134108 (2015).

[7] R. Juchtmans, G. Guzzinati, and J. Verbeeck, Extension of Friedel's law to vortex-beam diffraction, Phys. Rev. A **94**, 033858 (2016).

[8] J. Komrska, Fraunhofer diffraction at apertures in the form of regular polygons I, Opt. Acta **19**, 807 (1972).

[9] J. Komrska, Fraunhofer diffraction at apertures in the form of regular polygons II, Opt. Acta **20**, 549 (1973).

[10] J. Komrska, Simple derivation of formulas for Fraunhofer diffraction at polygonal apertures, J. Opt. Soc. Am. **72**, 1382 (1982).

[11] R. M. Sillitto, The structure of Fraunhofer diffraction patterns of apertures with N-fold rotational symmetry, Opt. Acta **30**, 1525 (1983).

[12] H. Kogelnik and T. Li, Laser beams and resonators, Appl. Opt. **5**, 1550 (1966).

[13] A. E. Siegman, *Lasers* (University Science Books, Mill Valley, CA, 1986), Chap 16.

[14] M. W. Beijersbergen, L. Allen, H. E. L. O. Vanderveen, and J. P. Woerdman, Astigmatic laser mode converters and transfer of orbital angular-momentum, Opt. Commun. **96**, 123 (1993).

[15] J. Vickers, M. Burch, R. Vyas, and S. Singh, Phase and interference properties of optical vortex beams, J. Opt. Soc. Am. A **25**, 823 (2008).

[16] J. Wang, J.-Y. Yang, I. M. Fazal, N. Ahmed, Y. Yan, H. Huang, Y. Ren, Y. Yue, S. Dolinar, M. Tur, and A. E. Willner, Terabit free space data transmission employing orbital angular momentum multiplexing, Nat. Photon. **6**, 488 (2012).

[17] S. Roychowdhury, V. K. Jaiswal, and R. P. Singh, Implementing controlled NOT gate with optical vortex, Opt. Commun. **236**, 419 (2004).

[18] G. Gibson, J. Courtial, M. Padgett, M. Vasnetsov, V. Pasko, S. Barnett, and S. Franke-Arnold, Free-space information transfer using light beams carrying orbital angular momentum, Opt. Express **12**, 5448 (2004).

[19] *Structured Light and Its Applications: An Introduction to Phase-Structured Beams and Nanoscale Optical Forces*, edited by D. L. Andrews (Elsevier, Cambridge, 2011).

[20] D. P. Ghai, P. Senthilkumaran, and R. S. Sirohi, Single-slit diffraction of an optical beam with phase singularity, Opt. Lasers Eng. **47**, 123 (2009).

[21] Q. S. Ferreira, A. J. Jesus-Silva, E. J. S. Fonseca, and J. M. Hickmann, Fraunhofer diffraction of light with orbital angular momentum by a slit, Opt. Lett. **36**, 3106 (2011).

[22] J. M. Hickmann, E. J. S. Fonseca, W. C. Soares, and S. Chavez-Cerda, Unveiling a Truncated Optical Lattice Associated with a Triangular Aperture Using Light's Orbital Angular Momentum, Phys. Rev. Lett. **105**, 053904 (2010).

[23] J. G. Silva, A. J. Jesus-Silva, M. A. R. C. Alencar, J. M. Hickmann, and E. J. S. Fonseca, Unveiling square and triangular optical lattices: A comparative study, Opt. Lett. **39**, 949 (2014).

[24] A. Ambuj, H. Shiau, M. Lucini, R. Vyas, and S. Singh, Effect of quadratic radial variation of phase on single slit diffraction of Laguerre-Gauss vortex beams, J. Mod. Opt. **59**, 1232 (2012).

[25] A. Ambuj, R. Vyas, and S. Singh, Diffraction of orbital angular momentum carrying optical beams by a circular aperture, Opt. Lett. **39**, 5475 (2014).

[26] A. Mourka, J. Baumgartl, C. Shanor, K. Dholakia, and E. M. Wright, Visualization of the birth of an optical vortex using diffraction from a triangular aperture, Opt. Express **19**, 5760 (2011).

[27] L. Clark, G. Guzzinati, A. Béché, A. Lubk, and J. Verbeeck, Symmetry-constrained electron vortex propagation, Phys. Rev. A **93**, 063840 (2016).

[28] E. Walla, C. Shaji, R. Vyas and S. Singh, Degeneracy in the diffraction of orbital angular momentum carrying beams, Opt. Lett. **43**, 5833 (2018).

[29] A first account of results of this paper was presented in A. Ambuj, R. Vyas, and S. Singh, Diffraction of Laguerre-Gauss vortex beams by regular polygons, in *Frontiers in Optics 2014*, OSA Technical Digest (online) (Optical Society of America, Washington, DC, 2014), Paper JTu3A.10.

[30] F. Gori, G. Guattari, and C. Padovani, Bessel-Gauss beams, Opt. Commun. **64**, 491 (1987).

[31] A. Hakola, S. C. Buchter, T. Kajava, H. Elfstrom, J. Simonen, P. Paakkonen, and J. Turunen, Bessel-Gauss output beam from a diode-pumped Nd:YAG laser, Opt. Commun. **238**, 335 (2004).

[32] Miguel A. Bandres and Julio C. Gutiérrez-Vega, Ince-Gaussian beams, Opt. Lett. **29**, 144 (2004).

[33] G. A. Siviloglou, J. Broky, A. Dogariu, and D. N. Christodoulides, Observation of Accelerating Airy Beams, Phys. Rev. Lett. **99**, 213901 (2007).

[34] J. Durnin, J. J. Miceli Jr., and J. H. Eberly, Diffraction-free Beams, Phys. Rev. Lett. **58**, 1499 (1987).

[35] I. S. Gradshteyn and I. M. Ryzhik, *Table of Integrals, Series, and Products*, 4th ed. (Academic, New York, 1965), p. 973.

[36] NIST Digital Library of Mathematical Functions, http://dlmf.nist.gov/, Release 1.0.19 of 2018-06-22, edited by F. W. J. Olver, A. B. Olde Daalhuis, D. W. Lozier, B. I. Schneider, R. F. Boisvert, C. W. Clark, B. R. Miller, and B. V. Saunders, Chap. 8.

[37] C. Stahl and G. Gbur, Analytic calculation of vortex diffraction by a triangular aperture, J. Opt. Soc. Am. A **33**, 1175 (2016).

[38] R. Phillips and L. Andrews, Spot size and divergence for Laguerre Gaussian beams of any order, Appl. Opt. **22**, 643 (1983).

[39] G. Lenz, Far-field diffraction of truncated higher-order Laguerre-Gaussian beams, Opt. Commun. **123**, 423 (1996).